Mechanical Properties of Inner-Arm Dynein-F (Dynein I1) Studied With In Vitro Motility Assays

Norito Kotani,* Hitoshi Sakakibara,† Stan A. Burgess,‡ Hiroaki Kojima,† and Kazuhiro Oiwa*†
*Graduate School of Life Science, University of Hyogo, Harima Science Park City, Hyogo 6781297, Japan; †Kobe Advanced ICT Research Center, National Institute of Information and Communications Technology, 588-2 Iwaoka, Nishi-ku, Kobe 6512492, Japan; and ‡Institute of Molecular and Cellular Biology, Faculty of Biological Sciences, University of Leeds, Leeds LS2 9JT, United Kingdom

ABSTRACT Inner-arm dynein-f of *Chlamydomonas* flagella is a heterodimeric dynein. We performed conventional in vitro motility assays showing that dynein-f translocates microtubules at the comparatively low velocity of ~1.2 μm/s. From the dependence of velocity upon the surface density of dynein-f, we estimate its duty ratio to be 0.6–0.7. The relation between microtubule landing rate and surface density of dynein-f are well fitted by the first-power dependence, as expected for a processive motor. At low dynein densities, progressing microtubules rotate erratically about a fixed point on the surface, at which a single dynein-f molecule is presumably located. We conclude that dynein-f has high processivity. In an axoneme, however, slow and processive dynein-f could impede microtubule sliding driven by other fast dyneins (e.g., dynein-c). To obtain insight into the in vivo roles of dynein-f, we measured the sliding velocity of microtubules driven by a mixture of dyneins -c and -f at various mixing ratios. The velocity is modulated as a function of the ratio of dynein-f in the mixture. This modulation suggests that dynein-f acts as a load in the axoneme, but force pushing dynein-f molecules forward seems to accelerate their dissociation from microtubules.

INTRODUCTION

Cilia and flagella play roles in propelling unicellular organisms and spermatozoa through water, in transporting small particles over the surfaces of vertebrate respiratory and reproductive tracts, and in carrying food particles along filter-feeders' gills (1). In addition to their roles in motility, cilia and flagella serve a variety of sensory functions. Defects in these organelles are thus associated with diverse human diseases (references in Snell et al. (2), Pazour and Witman (3), and Marshall and Nonaka (4)). Therefore, it is important that we understand the structures and functions of cilia and flagella.

Coordinated beating and bend propagation of cilia and flagella are generated by active sliding of peripheral doublet microtubules driven by ensembles of various types of dyneins (5,6). We have been using *Chlamydomonas* flagella for studies of the structure and function of dyneins since many mutants of flagella or dyneins provide valuable experimental systems for study (6,7). However, even with *Chlamydomonas*, the axoneme is complex since at least 11 dynein heavy chains (three outer-arm, eight inner-arm) exist and each could play crucial and distinct roles in proper flagellar functions (5,6). Inner-arm dyneins, which are more important in flagellar movement than outer-arms, are composed of six monomeric (dyneins -a, -b, -c, -d, -e, and -g) and one heterodimeric (dynein-f) dyneins, each of which have distinct mechanical properties (5,8,9).

Dynein-f, also known as dynein I1 (8), is an inner-arm dynein complex comprising two different heavy chains, each >500 kDa, together with a number of intermediate and light chains (8,10). Each heavy chain contains the sites of ATP hydrolysis and microtubule binding and thus constitutes the fundamental motor unit. Studies on flagellar mutants of *Chlamydomonas* have showed that mutants either lacking dynein-f or exhibiting altered intermediate chain (IC138) phosphorylation patterns have defects both in flagellar waveform and phototaxis (11–13). Hence, dynein-f may play important roles in regulation of flagellar motility (13,14). However, the complexities of molecular organization of dynein-f and poor motility in vitro have hampered the progress in understanding the mechanism of this dynein (9,12). Our group has focused on this heterodimeric axonemal dynein, surveying appropriate conditions for its motility and examining its mechanical properties.

In this study, we described the molecular configuration of dynein-f revealed by negative stain electron microscopy and after single particle analysis. We then carried out conventional in vitro motility assays on dynein-f (9,12,15). We provide evidence that this dynein is processive with a high duty ratio (time spent attached to its microtubule track/total ATPase cycle time ratio). We further investigated effects of dynein-f on microtubule movements driven by other fast dyneins as a model for in vivo functions of dynein-f. The results suggest that dynein-f works as a source of internal drag, but its dissociation from microtubules could be accelerated by forces acting on it, which may provide insights into how dynein-f works within an ensemble of motors in the axoneme.

MATERIALS AND METHODS

Protein purification

Dyneins -f and -c were each isolated from flagella of an outer-armless mutant (*oda1*) of *Chlamydomonas reinhardtii* (strain 137c) as described (9,15) with

Submitted November 27, 2006, and accepted for publication April 6, 2007.
Address reprint requests to Kazuhiro Oiwa, oiwa@nict.go.jp.
Editor: Shin'Ichi Ishiwata.

0006-3495/07/08/886/09 $2.00
doi: 10.1529/biophysj.106.101964

some modifications. Coprecipitation of purified dynein-f with microtubules in the presence of 1 mM ATP did not show significant nonspecific binding of dynein-f to microtubules. Porcine brain tubulin, purified according to Vallee (16), was polymerized into microtubules in assembly buffer (1 mM $MgCl_2$, 1 mM EGTA, 1 mM guanosine triphosphate (GTP), 10% (v/v) dimethylsulfoxide, 80 mM PIPES (1,4-piperazinediethanesulfonic acid)/KOH, pH 6.9) at 37°C, and stabilized by adding 10 μM taxol. Dyneins and tubulin concentrations were determined using the Bradford assays.

Electron microscopy

The molecular configuration of dynein-f was investigated by electron microscopy with the negative staining technique (17,18). To improve the quality of negative staining, we eluted dynein-f from the final anion exchange column with buffer containing 30 mM MOPS (3-(*N*-morpholino)propanesulfonic acid), 5 mM $MgCl_2$, 1 mM EGTA, and 0.1 mM dithiothreitol (DTT), pH 7.4 (MMDE buffer) in a KCl gradient. Fresh stock dynein samples (~0.65 μM protein and ~300 mM KCl) were diluted to 20 nM into MMDE buffer containing 100 mM KCl and applied to carbon-coated grids treated with ultraviolet light as described (19), before staining with 1% aqueous uranyl acetate. Microscopy was performed on a JEM 2000EX (JEOL, Akishima, Japan) operating at 80 kV. Micrographs were taken at a nominal magnification of 40,000 times. Micrographs were digitized on either an Imacon Flextight 848 scanner (Imacon A/S, Copenhagen, Denmark) or an EPSON GTX-700 (Seiko Epson, Nagano, Japan). Digital micrographs were imported into the SPIDER suite of programs (20) for all subsequent image processing.

Measurement of basal Mg^{2+}-ATPase activity

Mg^{2+}-ATPase activity was measured using an enzyme coupling assay, in which inorganic phosphate (Pi) released from dynein ATPase was measured spectrophotometrically (Enzcheck, Molecular Probes, Eugene, Oregon) (21). We added 0.5–1 μg/ml of dynein-f or dynein-c to HMDE solution containing 30 mM HEPES/NaOH (pH 7.4), 5 mM $MgSO_4$, 1 mM DTT, 1 mM EGTA, and various concentrations of ATP (1 μM to 0.99 mM), incubated at 25° ± 1°C, and continuously monitored the absorbance at 360 nm. Although we did not control the ADP concentrations in these measurements, care was devoted to dynein concentrations to ensure that steady-state conditions were achieved.

In vitro motility assays

In vitro assays were performed at 24° ± 2°C, basically as described (15) with some modifications. A flow cell, volume 10 μl, was made from a glass slide (No. 1 glass slide, 26 mm × 76 mm, S-1126, Mastunami Glass Ind, Osaka, Japan) and a coverslip (No. 1, 18 mm × 18 mm, Matsunami Glass Ind) after the glassware had been cleaned with the solution containing 0.1 M HCl and 70% ethanol and rinsed with distilled water. Purified dyneins -c and -f (200–400 μg/ml) were diluted to various concentrations in the HMDE solution containing 150 mM HEPES/KOH (pH 7.4), 5 mM $MgSO_4$, 1 mM DTT, 1 mM EGTA, and 0.5 mg/ml bovine serum albumin. For landing rate assays and velocity measurements at various concentrations of ATP, we used the HMDE solution containing 30 mM HEPES/NaOH instead of 150 mM HEPES/KOH. The flow cell was filled with 10 μl of the diluted dynein solution, incubated for 5 min, and washed with buffer solution. After washing the flow cell with buffer solution containing 40 μg/ml microtubules, 1 mM DTT, various concentrations of ATP (from 10 μM to 1 mM) and the ATP regenerative system containing 0.02 mg/ml creatine kinase and 5 mM phosphocreatine, were infused into the flow cell. For the landing rate assays, we added 0.05% (w/v) methylcellulose to the buffer. Lateral diffusion of microtubules near the glass surface in the above solution was measured, and the coefficient of a 10-μm-long microtubule was found to be 0.12 $\mu m^2/s$.

Microtubule movement was observed and recorded with a dark-field optical microscope (BHF, Olympus, Tokyo, Japan), equipped with a high numerical aperture dark-field condenser (BH-DCW, Olympus), and a charge-coupled device camera (C2400-77H, Hamamatsu Photonics, Hamamatsu, Japan). The images were recorded on VHS videotape with a frame rate of 30 Hz. Video tapes of the microtubule movement were played back off-line, and positions of individual microtubules were digitized frame by frame using a frame-grabber and a computer with a precision of 0.10 ± 0.04 μm. Microtubule displacement was calculated and plotted with respect to time. Trajectories were processed with the moving average, and the derivatives with respect to time were calculated. To obtain reliable velocities, only microtubules longer than 2 μm in length (mean length = 5.4 ± 2.0 μm, $n = 134$) that moved continuously over their lengths were analyzed.

For the landing rate assay (15,22,23), the dark-field optical microscope was used to enable precise scoring of landing filaments as those that had touched down and moved for longer than 0.8 μm at 0.5 mM ATP at constant tubulin concentration (40 μg/ml). The mean length of microtubules used in this assay was 9.0 ± 3.6 μm ($n = 131$). In our previous study on dynein-c (15), we directly determined the surface density of active dynein-c molecules from each dynein concentration using a single-molecule technique (24), and we showed that surface densities measured by this technique were 10-fold less than estimated by assuming that all dynein molecules in the solution bound to the surface. However, in this study we calculated each surface density of dynein-c and dynein-f assuming that all dynein molecules infused into the flow cell evenly attached to the surface of the flow-cell.

Optical trap nanometry

The force-velocity relation of ensembles of dynein-c molecules was obtained using optical trap nanometry. The experimental setup for the optical trap was basically the same as described previously (15,25). For detection of small beads (300 nm in diameter), we adopted the dark-field illumination and extended the single molecule measurements (25) to the ensemble.

Protein-G-coated polystyrene carboxylated beads (300 nm in diameter) were incubated with 2 mg/ml of antitubulin antibody (Sigma T9028, St. Louis, MO) on ice in assay buffer (5 mM $MgSO_4$, 1 mM EGTA, 1 mM DTT, 150 mM HEPES/KOH, pH 7.4) for 3 h. The beads were then mixed with taxol-stabilized microtubules and incubated for 30 min. After introducing the bead-microtubule complexes into a flow cell, we then captured the resultant bead-microtubule complexes by the optical trap. We brought the free end of the microtubule to within 3 μm of the dynein-c-coated surface (density of dynein-c was 160 molecules/μm^2), allowing the microtubule to engage the dynein surface. As dynein-c pulled the microtubule, the bead was displaced in the optical trap. Displacement of the bead was measured using a quadrant photodiode system with 0.1-nm spatial (noise equivalent value) and 0.24-ms temporal resolution. Trap stiffness (20 fN/nm) was determined from variances of the Brownian fluctuations of beads.

The force-velocity relation of the ensemble of dynein-c was determined as follows: 2–5 runs of the bead displacement were classified with respect to their give forces, and the high frequency components were reduced with a low-pass filter ($f_c = 100$ Hz). Each displacement was separated into segments, each covering 20 ms, and the slope of each segment was calculated as the velocity at the corresponding force. The velocities thus obtained were averaged with respect to the displacement, which corresponds to force.

RESULTS

Molecular configuration of dynein-f

We confirmed by polyacrylamide gel electrophoresis that dynein-f has two distinct heavy chains, three intermediate chains, and several light chains (Fig. 1 *A*). Negative staining electron microscopy shows that molecules of dynein-f are sparsely distributed on the carbon grid with no indication of aggregation. Dynein-f is thus dimeric, even when purified by

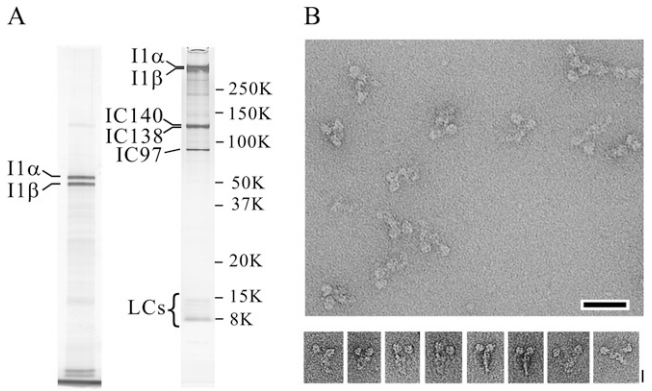

FIGURE 1 Purification and molecular morphology of dynein-f. (*A*) sodium dodecyl sulfate-polyacrylamide gel electrophoresis (*left lane*: 3% polyacrylamide, *right lane*: 5%–20%) of purified dynein-f, whose heavy chains (I1α and I1β) run at 450 kDa. Three intermediate chains (IC140, IC138, and IC97) are clearly visible in the gel. A few light chains (LCs) are also visible. (*B*) Field of negatively stained dynein-f molecules in the absence of nucleotide showing tails attached to two globular heads. Scale bar, 50 nm. Gallery of typical molecules showing the two-headed configuration. Scale bar, 20 nm.

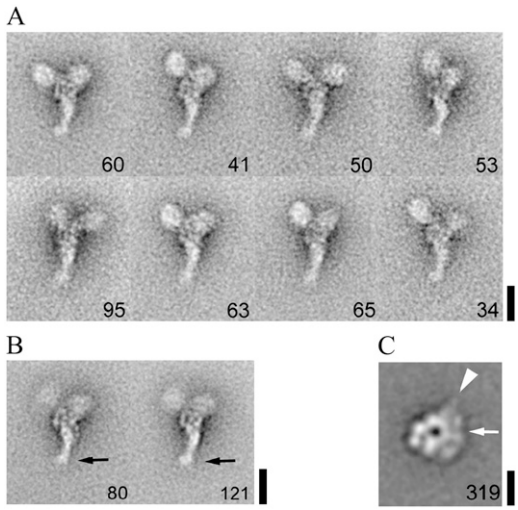

FIGURE 2 Structure of dynein-f. (*A*) Class averages showing a variety of head-head configurations (*upper* two globular domains) and the asymmetric tail domain (*pointing downwards*). (*B*) Class averages showing substructural detail within the tail domain. A small distal domain is indicated (*arrow*). (*C*) Class average showing the head domain after a second round of alignment using just the part of each image containing the head. This class is strikingly similar to right views of dynein-c in the absence of nucleotide (17), and the corresponding positions of dynein-c's stalk (*arrowhead*) and tail (*arrow*) domains are indicated. The number of images in each class is shown in the lower right corner. The number of individual molecules aligned and classified is $n = 578$ (*A* and *B*) and $n = 1566$ (*C*). Scale bar, *A* and *B*: 20 nm, *C*: 10 nm.

ionic exchange chromatography. Close inspection shows two head domains attached together by an elongated tail (Fig. 1 *B*). The distance between the two heads is quite variable, as is the structure of the tail. Single particle image analysis confirms this organization and reveals new substructure of the molecule (Fig. 2 *A*). Despite considerable variability in the spatial arrangement of the two heads among all individual molecules examined, several classes show a surprisingly characteristic structure in which the two heads are relatively closely apposed at one end of a tail structure that itself has a characteristic asymmetric structure (Fig. 2 *B*). This asymmetric organization could potentially be used as a marker to distinguish α and β heads (although we have not attempted this here). Substructure within the tail domain probably corresponds to each of the tail domains of the heavy chains together with their intermediate and light chains. A prominent domain at the distal end of the tail (*arrow*, Fig. 2 *B*) is evident.

Alignment of the head domains of negatively stained molecules clearly shows them to comprise an asymmetric ring-like morphology (Fig. 2 *C*) very similar to that of another *Chlamydomonas* flagellar inner arm subspecies, dynein-c reported previously in the so-called right view (17,18). This confirms the interpretation of head-head-tail organization made from the whole molecules and also the structural conservation between dynein-f and dynein-c. The point of emergence of the tail is not seen in these images, presumably owing to conformational variability on the grid under these imaging conditions and to the small number of molecules in this data set. However, its location is indicated based on the known position of the tail of dynein-c (*arrow* Fig. 2 *C*). The stalk, with its distally located microtubule-binding domain, is not observed in these samples, probably owing to its small size and flexibility. Its likely position is indicated (*arrowhead*, Fig. 2 *C*).

Basal ATPase activity of dynein-f

To characterize enzymatic properties of heterodimeric dynein-f, we performed steady-state kinetic analyses of dynein-f. Its basal ATPase rate showed Michaelis-Menten-type kinetics, with K_m for ATP $= 3.3 \pm 0.7$ μM and $v_{max} = 3.3 \pm 0.2$ s^{-1} head^{-1} (Fig. 3). The basal ATPase rate of dynein-c measured under the same conditions as dynein-f showed Michaelis-Menten-type kinetics, with K_m for ATP $= 31.4 \pm 1.1$ μM and $v_{max} = 4.4 \pm 0.04$ s^{-1} head^{-1}. Thus, the Mg-ATPase of dynein-f under steady-state conditions is characterized by a high v_{max} even without microtubules as reported in other dyneins (26–28) but a fairly low K_m compared to dynein-c. Deviations of the ATPase data from the Michaelis-Menten equation were obvious especially at low concentrations of ATP. Although the deviations might reflect distinct ATPase activities of each head, it is not easy to assign the deviations to the roles of each head, given that each one has at least four nucleotide-binding sites.

Rate of landing of microtubules onto dynein-f-coated surfaces

We measured the rate at which microtubules came out of the bulk solution and then landed on and moved more than

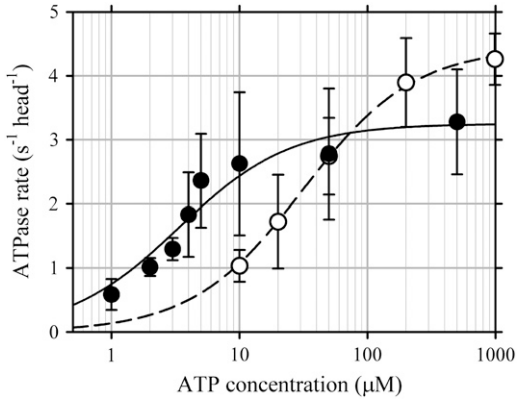

FIGURE 3 ATPase rate of dynein-f. Basal ATPase activities of dynein-f (*solid circles*) and -c (*open circles*) at various ATP concentrations. Error bars indicate standard deviations. The curves are fits by the Michaelis-Menten equation: maximum ATPase rate, $v_{max} = 3.3 \pm 0.2$ s^{-1} head^{-1} and $K_m = 3.3 \pm 0.7$ μM for dynein-f (*solid curve*): $v_{max} = 4.4 \pm 0.04$ s^{-1} head^{-1}, and $K_m = 31.4 \pm 1.1$ μM for dynein-c (*dashed curve*).

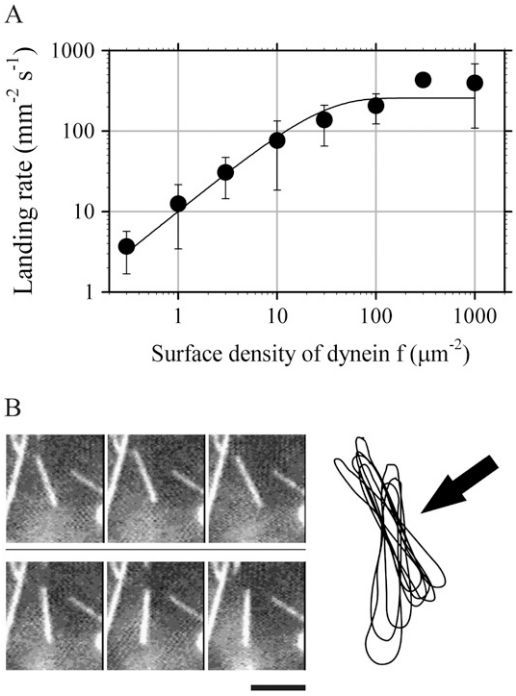

FIGURE 4 Dependence of microtubule landing rate on the density of dynein-f-coated glass surfaces. (*A*) The solid curve is the fit to the Poisson model for a single molecule of dynein-f sufficing to move a microtubule: $k(\rho) = C_0 (1 - e^{-A\rho})$, where $k(\rho)$ is landing rate at dynein-f density ρ and A is the product of microtubule length and twice the reach of dynein-f; these values are $C_0 = 260$ mm^{-2} s^{-1}, $A = 0.04$ μm^2. (*B*) Video sequence and tracings of images showing thermally driven rotation of a microtubule around a nodal point while also moving progressively (dynein-f density: 1 molecule per μm^2). Tracings were obtained from successive video images at 1/3-s intervals. The arrow indicates the fixed point on the surface, about which the microtubule rotated. Scale bar, 5 μm.

0.8 μm over surfaces coated with dynein-f (a displacement of <0.8 μm is difficult to distinguish from Brownian motion). Landing and movement of microtubules was observed even at densities of a few molecules per 10 μm^2. The rate plotted against surface density of dynein-f (Fig. 4) is well fitted by the theoretical relationship for a single dynein-f molecule being sufficient for attachment and movement of microtubules (22). The area in which a microtubule can interact with dynein molecules (0.04 μm^2) was in the same order as that of dynein-c (0.34 μm^2 divided by 10), and the maximal landing rate (260 mm^{-2} s^{-1}) was the same as that measured on a dynein-c-coated surface (15).

Most microtubules (>70%) observed at very low surface densities of dynein-f (below one molecule per μm^2) rotated erratically about a vertical axis through a fixed point on the surface. When its trailing end reached this nodal point, the microtubule dissociated from the surface and diffused back into solution. These observations are consistent with a single processive motor molecule being located at the nodal point. At higher dynein-f densities, microtubules exhibited negligible rotation when moving, presumably because they were constrained laterally by the attachment to additional dynein-f molecules.

Sliding movement of microtubules driven by dynein-f

To characterize the mechanical properties of dynein-f, we used the conventional in vitro motility assays (9,12,15) in which microtubules glide over glass surfaces coated with dynein-f at a surface density of 1000 molecules per μm^2. The movement of microtubules driven by dynein-f was highly dependent on the surface conditions. We examined several types of surfaces: borosilicate glass, spin-on glass (Tokyo Ohka Kogyo, Kawasaki, Japan), borosilicate glass cleaned with an anionic detergent, and the same glass cleaned with a plasma cleaner. As far as we have examined, we found that dynein-f retains its motile activity when bound to borosilicate glass that had been washed with 0.1 M HCl and 70% ethanol but it does not on other surfaces. On this glass surface, microtubules were moving smoothly over a distance of longer than 50 μm. Some axonemal dyneins have been reported to have an ability to rotate a microtubule while driving it forward (9). However, we have not observed distinct rotation of microtubules moving on the dynein-f-coated surface.

Sliding velocities of microtubules depended on the ATP concentration in a Michaelis-Menten-like manner: K_m for ATP was 55 $\pm$ 11 μM and V_{max} was 1.6 $\pm$ 0.1 μm/s (Fig. 5). Although this maximum sliding velocity of microtubules is the fastest among those reported for dynein-f (9,12), it is still slow compared with the estimated velocity of microtubules in the axoneme (14) and only one-fifth to one-tenth of that observed for inner-arm dynein-c under the same conditions.

We measured the relationship between the surface density and sliding velocity in the presence of 500 μM ATP and show that the sliding velocity of microtubules depends slightly

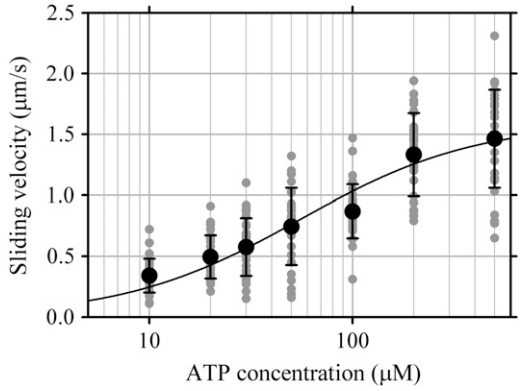

FIGURE 5 ATP concentration dependence of sliding velocity of microtubules on dynein-f-coated surfaces. Error bars indicate standard deviations for velocities. The curve is a fit by the Michaelis-Menten equation: the curve has maximal gliding velocity, $V_{max} = 1.6 \pm 0.1$ μm/s, and $K_m = 55 \pm 11$ μM. Gray dots indicate original data.

upon the surface density of dynein-f. The ratio of the sliding velocity of a microtubule driven by a single dynein-f molecule to the maximal velocity attained at saturating dynein density provides the duty ratio (29). In the case of this dynein-f sample, the velocity at 0.3 molecules per μm^2 is 0.62 ± 0.32 μm/s, the velocity at 1000 molecules per μm^2 is 0.99 ± 0.37 μm/s providing a duty ratio of 0.63 (Fig. 6).

Microtubule sliding upon surfaces coated with dynein-f and -c at various ratios

If slow dynein-f imposes an internal load on other faster dyneins in vivo, it would be possible to estimate the internal load generated by dynein-f by using an in vitro motility assay. There are similar arguments in smooth muscle myosin about whether the degree of 20-kDa light chain phosphorylation may modulate the rate of the cross-bridge cycle (30). Since the contractile response in smooth muscle is complex, experiments to unravel this complexity were performed in vitro (31,32). Thus, we follow this strategy: to get insight into the roles of dynein-f in an axoneme, we experimentally reconstituted the conditions in the axoneme by mixing the fast dynein (dynein-c) with dynein-f in an in vitro motility assay. We assumed that all dynein molecules in the experimental buffer settled down on the surface and kept their activities intact. Density of total dynein molecules was kept constant (1000 molecules/μm^2), and the mixing ratio of dynein-f to the total varied 0%–100%. At 0% and 100% of mixing ratio of dynein-f, microtubules move smoothly and continuously over the surface at velocities of 8.0 ± 1.8 μm/s and 1.2 ± 0.5 μm/s, which correspond to the velocity of dynein-c alone and dynein-f alone, respectively.

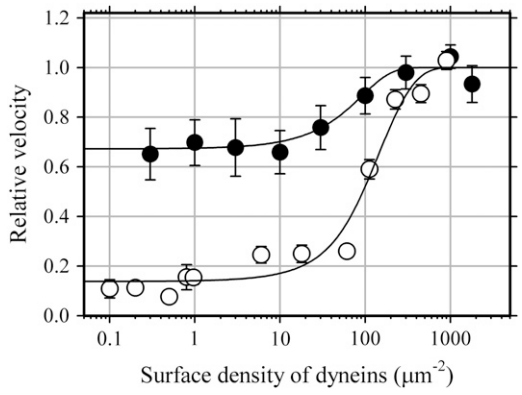

FIGURE 6 Relationship between velocity of microtubule sliding and surface density of dynein. Error bars indicate standard deviations for dynein-f (*solid circles*) and dynein-c (*open circles*). Solid curves are fits to $V_{max}(1 - e^{-A\rho f})/(1 - e^{-A\rho})$ in which V_{max}, ρ, f, and A are, respectively, the maximal velocity, the density of dyneins, the duty ratio, and the product of microtubule length and twice the reach of a dynein molecule; values: for dynein-f $V_{max} = 0.99 \pm 0.37$ μm/s, $V_{min} = 0.62 \pm 0.32$ μm/s, $f = V_{min}/V_{max} = 0.63$, $A = 0.027 \pm 0.01$ μm^2 and for dynein-c $V_{max} = 5.1$ μm/s, $V_{min} = 0.7$ μm/s, $f = V_{min}/V_{max} = 0.14$, $A = 0.053$ μm^2. The data for dynein-c are replotted from Sakakibara et al. (15).

On surfaces coated with a mixture of dynein-c and -f, we focused on microtubules with a length longer than 2 μm and shorter than 11 μm. These microtubules showed continuous and smooth movement at intermediate velocities between that of dynein-c alone and dynein-f alone. The trajectories of microtubules show that the movement is uniform over the surface and the velocity is almost constant (Fig. 7 *A*). The distributions of microtubule velocities at all mixing ratios were unimodal (no bimodal distributions were seen) (*gray solid circles* in Fig. 7 *B*). These results suggest that dynein-f and dynein-c do not form patches on the surface but are evenly mixed and distributed, within the range of microtubule lengths used here.

The sliding velocity of microtubules decreases linearly as the ratio of dynein-f in the mixture increases (Fig. 7 *B*). Since dynein-c has a low duty ratio (0.14, (15)), the sliding velocity of microtubules driven by dynein-c is a function of the number of dynein-c capable of interacting with a microtubule and the duty ratio (the *solid curve* in Fig. 7 *B*). However, the decrease in velocity we observed is much larger than the decrease caused by the density of dynein-c, so that dynein-f must be acting as a drag to slow down the velocity at which microtubules are moved by the faster dynein-c.

Force-velocity relationship of dynein-c measured with optical trap nanometry

The evaluation of drag force of dynein-f requires the force-velocity relationship of microtubule sliding driven by the ensemble of dynein-c (see Discussion). Microtubules attached to polystyrene beads were captured by the optical trap and brought into contact with the dynein-c-coated surface. Those microtubules interacting with the dynein surface showed transient movements (Fig. 8 *A*). Beads were pulled by microtubules for various periods and were then drawn rapidly back to the trap center, whereupon the microtubules rebound to the surface and began to move beads again.

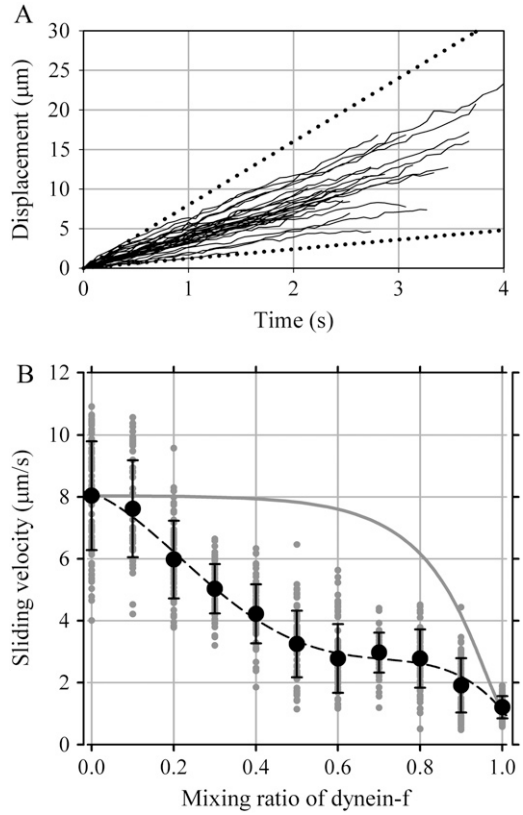

FIGURE 7 Microtubule sliding driven by mixtures of dyneins -f and -c. (*A*) Trajectories of individual microtubules driven by dynein-f and -c at a mixing ratio of 0.5 were plotted as a function of time. Dotted lines indicate the displacements with constant velocity of 8 (*upper*, corresponding to the maximal velocity driven by dynein-c alone) and 1.2 (*lower*, corresponding to the maximal velocity driven by dynein-f alone) μm/s, which correspond to the maximal velocity driven by dynein-c and dynein-f, respectively. (*B*) Sliding velocities for mixtures of dynein-f and -c. Error bars indicate standard deviations. The gray solid line is the estimated velocity driven by dynein-c alone. Gray solid circles are raw data points at various mixing ratios. The distributions indicate unimodal distributions of velocity at each mixing ratio. The dashed curve is the quartic equation to describe the relation. The coefficient of determination, the measure of how well a regression model describes the data, was 0.998.

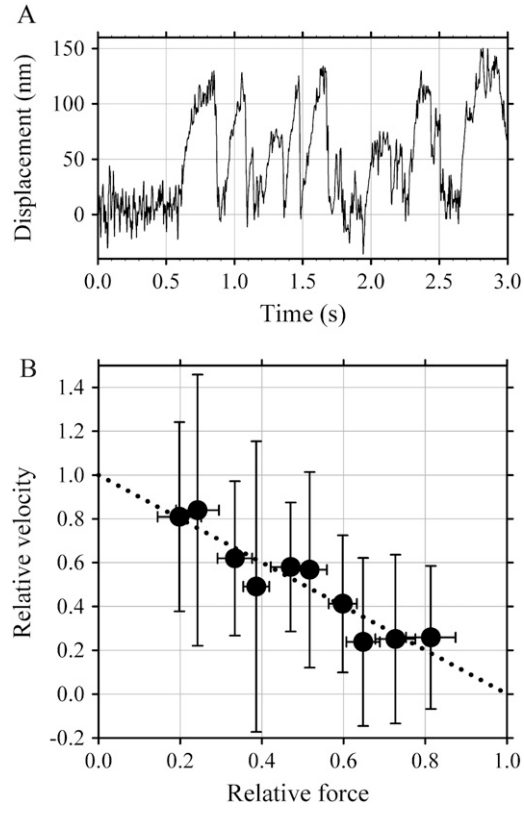

FIGURE 8 The force-velocity relationship of microtubule sliding driven by ensembles of dynein-c. (*A*) A typical record of force and movement of a microtubule driven by ensembles of dynein-c in the presence of 200 μM ATP. (*B*) The force-velocity curve was almost linear: i.e., the velocity decreased linearly with increasing load. Since the microtubules often dissociate before slowing down substantially, the force-velocity curves do not reach the force axis (zero velocity). A linear fit to the data gives an extrapolated maximal velocity of 1.5 μm/s, agreeing with those for microtubule's gliding measured in in vitro motility assays.

The force-velocity relationship was almost linear: i.e., the velocity decreased linearly with increasing load (Fig. 8 *B*). These features were generally consistent with those of the force-velocity curve of single dynein-c molecules moving on a microtubule (25).

DISCUSSION

Structure and motility of dynein-f

Despite our understanding of the molecular composition and localization of dynein-f in the axoneme (10,33), its structure and motility has not been well characterized. Dynein-f has shown only 'poor' movement of microtubules in in vitro motility assays: the velocity of microtubules were observed in the range between 0 and 0.7 μm/s, which is much slower than that of other axonemal dyneins and the calculated maximal velocity of microtubule sliding in an axoneme (9,12). As Smith and Sale (12) indicated, there are at least three possibilities for the immotile or poor activity of dynein-f. First, isolation or the motility assay itself spoils dynein-f's motility. Second, the activity of dynein-f is regulated through mechanisms such as phosphorylation of the intermediate chain, IC138. Third, the slow movement of dynein-f is its intrinsic property and plays some important and yet to be identified role in the axoneme.

Dynein-f purified in this study contains two distinct heavy chains, three intermediate chains, and major light chains as reported (9,12). Though we could not identify all light chains, the molecule appears to remain intact. Thus, negative stain electron microscopy and single particle image processing establish that the purified particles are two-headed molecules with each head resembling that of dynein-c prepared under the same conditions (17) and the molecule retains basal ATPase activity.

The 138-kD intermediate chain, which was fully phosphorylated in vitro by the casein kinase, had such a different mobility in a urea gel from dephosphorylated IC138 that we can estimate its content. However, native IC138 showed a smear band in the gel, so that we could not examine the degree of IC138 phosphorylation of our dynein samples. It was reported that reconstitution of dynein-f with axonemes bearing radial spokes resulted in dephosphorylation of the IC138 (11). Thus, the IC138 of dynein-f purified from *oda1* in this study is probably dephosphorylated. We have also found that the IC138-phosphorylation we carried out with casein kinase did not have significant effects on in vitro motility of dynein-f (H. Sakakibara, W. Sale, and K. Oiwa, manuscript in preparation). The dynein-f we prepared probably has a low degree of phosphorylation and would seem to be an active dynein.

In vitro motility of dynein-f depended highly upon the surface conditions. We have explored several methods for cleaning and coating the glass surface and found suitable conditions for motility. However, even under these surface conditions, dynein-f displayed only slow movement of microtubules ($\sim$1.2 μm/s). Although we may not have found the best conditions, the slow movement may well be an intrinsic property of dynein-f.

In this study, to our knowledge, the electron microscope images provide the most detailed views to date of dynein-f and indeed of any two-headed dynein species. Quick-freeze deep-etch electron microscopy has been used previously to visualize several purified inner-arm species of *Chlamydomonas* (34). Peak 5 of their HPLC chromatogram of high-salt extracts from axonemes corresponds to the dynein-f fraction in our preparation. Dynein molecules in peak 5 possess two globular heads with long tails. The tails are extremely variable in these preparations and appear to interact with each other only at their distal ends, suggesting that the complex is splayed out on the mica surface adopting many different configurations (34). That the tail domain in this study shows a well-defined structure and appears to comprise a more intimate association of the two-tail domains suggests that the structural preservation here is more complete than in the earlier study. The heads seen in images of whole molecules (Figs. 1 and 2 *A*) resolve into ring-like structures (Fig. 2 *C*) characteristic of a particular view of the head domain of dynein-c. This resemblance in head structure indicates the organizational similarity between dynein-f and dynein-c subspecies, which perhaps is common to all dynein isoforms (axonemal and cytoplasmic). It also establishes that the remaining structure, the tail, must contain the remaining portion of the two heavy chains (so-called tail domains) together with their accessory intermediate and light chains. Further structural studies, perhaps employing cryoelectron microscopy to avoid surface adsorption-induced structural rearrangements, will be required to understand the structure of this two-headed dynein in more detail.

The two heads of negatively stained dynein-f are spread apart, possibly due to interactions between the molecules and the carbon film to which they are bound. Dynein-f (I1) in electron tomograms (33) and in longitudinal sections of flagellar axonemes (10,35,36) shows a similar separation between the two heads. This is in contrast to outer arm dyneins, which show a more intimate association between heads, appearing stacked upon one another (33,37), or cytoplasmic dyneins (38). Dynein-f may work in a different manner from either outer arm dyneins or cytoplasmic dyneins, being designed to hold on but not to move very fast (see below).

Mechanical properties of dynein-f

Our in vitro studies of dynein-f demonstrate that landing rates of microtubules follow the theoretical relationship for a single dynein molecule being sufficient for attachment and motility of microtubules (22). At low surface densities, continuous movement of a microtubule appears to be sustained by a single dynein-f molecule. Surface-density dependence of microtubule sliding velocity suggests that the two-headed dynein-f motor has a high duty ratio (0.63). Based upon these observations, we conclude that dynein-f is a processive motor.

Although processivity of axonemal dyneins in vitro has been reported in an outer-arm dynein (39) and in a single-headed inner-arm dynein (15), it is not clear why this is necessary for microtubule sliding in situ (i.e., in an axoneme). During normal swimming movements, *Chlamydomonas* flagella generate bending waves with a rate of sliding in principal bends of 7.3 radians/cycle with a typical beat frequency of $\sim$65 Hz (14). The average distance between adjacent double microtubules is 40 nm, and so the average peak-to-peak shear between adjacent doublet microtubules is estimated to be $\sim$280 nm. Thus the average sliding velocity between doublet microtubules is expected to be $\sim$18 μm/s (280 nm $\times$ 65 Hz). Under these circumstances slow processive dyneins may therefore impede, rather than assist, microtubule sliding driven by the ensemble of relatively faster dyneins with low-duty ratios.

To evaluate the effect of dynein-f on microtubule sliding in situ, we performed the mixing experiments and compared the velocity that was calculated from the duty ratio of dynein-c to the velocity experimentally obtained. The velocity of microtubules driven by dynein-c without impedance of dynein-f was calculated:

$$V_c = V_{c\_max}\{1 - \exp(-A \times \rho \times f)\}/\{1 - \exp(-A \times \rho)\},$$

where ρ is the density of dynein-c, f is the duty ratio, and A is the effective area of dynein-c, 0.034 μm^{-2}. The velocities measured ($V_{measured}$) at all mixing ratios were lower than those estimated according to the above equation. The force-velocity relationship of dynein-c in ensembles (Fig. 8 *B*) and at a single molecule level (25) obtained through optical trap experiments showed that the velocity decreases linearly as the load is increased. Thus, a reduction of velocity ($\Delta V = V_c - V_{measured}$) can be converted into the load (F) on dynein-c

with a proportionality factor, α, and the mixing ratio of dynein-c $(1 - r)$ and dynein-f (r), i.e., $F = \alpha \times \Delta V \times (1 - r)/V_c$. In this study the force generated by dynein-c can be assumed to be balanced by the drag force generated by dynein-f. Thus, we estimated a drag coefficient (c) of a dynein-f molecule at various velocities ($c = F/V_{measured}$/r). Although errors of the estimation were rather large, the drag coefficient shows the tendency to steeply increase in the low velocity range (<3 μm/s), reach a peak, and then decrease gradually as velocity increases (>4 μm/s) (Fig. 9). This relation suggests that dynein-f in situ might work as a force generator in the low velocity range (<2 μm/s) but disengage (dissociates rapidly from microtubules) when pushed forward in the fast velocity range (>4 μm/s). The alternative explanation is that the number of dynein-f molecules which are engaged in active force generation decreases when the microtubule moves faster than 4 μm/s. Such strain-sensitive behavior might be a crucial function of dynein-f in situ.

The possible roles of dynein-f in situ

Wave-form analysis of mutant *Chlamydomonas* flagella has shown that a mutant lacking dynein-f (*pf 30*) has a reduced shear amplitude for the forward mode bending pattern without significant reduction of beat frequency (14). The equation of flagellar motion balances the moments due to the internal elasticity, the internally produced active moments (i.e., the dynein-generating active moments), and the moments due to the viscous drag of the external fluid (40). Since the elastic bending moment was taken as proportional to the local curvature, the reduction of shear angle means a decrease in the elastic bending moment. Therefore, a small reduction in beat frequency and a reduction in shear angle suggest that the active moment generated by dynein decreases and balances the rather small bending moment. Taken together, we suggest that slow dynein-f motors are engaged in force generation at low velocities and contribute mainly to the generation of active moments in the fully developed bend.

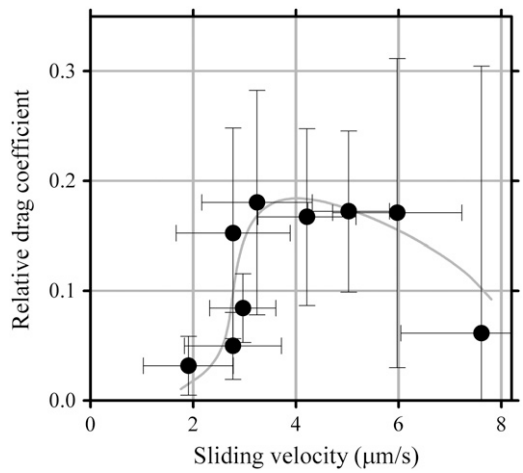

FIGURE 9 Relative drag coefficient of dynein-f calculated as a function of velocity. As shown in Fig. 7, the reduction of the velocity of microtubules driven by dynein-c is due to the presence of dynein-f. Based upon the linear force-velocity relation of dynein-c in Fig. 8 and the previous study (25), the reduction of the velocity is converted into the load on dynein-c. We calculated the relative drag coefficient of dynein-f by dividing the load by the velocity measured and the mixing ratio of dynein-f and then plotted this coefficient with respect to microtubule sliding velocity. Error bars indicate standard deviations. The gray curve is obtained using the fit of a quartic equation to the relationship between the velocity and the density of dynein-f (Fig. 7, *dashed curve*).

Since dynein-f and dynein-c also show processivity, this implies that in an axoneme they operate not only to translocate doublets but also to hold them together long enough for an episode of active bending. This property, which may correspond to ''adhesion'' in the geometric clutch hypothesis (41,42), provides force that the transverse force must overcome to ''switch off'' (terminate) an episode of dynein engagement (41,42). The properties reported for dynein-f would make it especially suited to provide this property of adhesion. Defects in dynein-f reduce the amount of curvature that develops in the beat of an intact flagellum (14). This is possibly because a reduction in adhesion between the doublets will cause the dyneins to switch ''off'' prematurely before a normal amount of bending develops.

The strain-dependent detachment rate of dynein-f suggests that a structural component that is capable of limiting sliding resides in these dyneins. In addition, this strain-sensitive detachment could cause a cooperative detachment of other dynein molecules from their microtubules, leading to backward movement of the microtubule until enough strain is released to allow the dyneins to reengage. Such cooperativity may be a source of the oscillatory flagellar movement, and the conversion of microtubule sliding into rudimentary oscillatory bending waves may occur in small subsets of the axonemal structure. A detailed mechanism of dynein-f, however, will await further analysis using single-molecule techniques such as optical trap measurements.

We thank Dr. Yuji Shitaka for searching optimal conditions of in vitro motility assays. We also thank Ms. Yukako Sakai for technical support.

This work was supported by the Grant-in-Aid for Scientific Research on the Priority Area ''Regulation of Nano-systems in Cells'' by the Ministry of Education, Science, and Culture of Japan.

REFERENCES

1. Gibbons, I. R. 1981. Cilia and flagella of eukaryotes. *J. Cell Biol.* 91: 107s–124s.
2. Snell, W. J., J. Pan, and Q. Wang. 2004. Cilia and flagella revealed: from flagellar assembly in *Chlamydomonas* to human obesity disorders. *Cell.* 117:693–697.
3. Pazour, G. J., and G. B. Witman. 2003. The vertebrate primary cilium is a sensory organelle. *Curr. Opin. Cell Biol.* 15:105–110.
4. Marshall, W. F., and S. Nonaka. 2006. Cilia: tuning in to the cell's antenna. *Curr. Biol.* 16:R604–R614.
5. Kamiya, R. 2002. Functional diversity of axonemal dyneins as studied in *Chlamydomonas* mutants. *Int. Rev. Cytol.* 219:115–155.

6. DiBella, L. M., and S. M. King. 2001. Dynein motors of the *Chlamydomonas* flagellum. *Int. Rev. Cytol.* 210:227–268.
7. Pazour, G. J., N. Agrin, J. Leszyk, and G. B. Witman. 2005. Proteomic analysis of a eukaryotic cilium. *J. Cell Biol.* 170:103–113.
8. Piperno, G., Z. Ramanis, E. F. Smith, and W. S. Sale. 1990. Three distinct inner dynein arms in *Chlamydomonas* flagella: molecular composition and location in the axoneme. *J. Cell Biol.* 110:379–389.
9. Kagami, O., and R. Kamiya. 1992. Translocation and rotation of microtubules caused by multiple species of *Chlamydomonas* inner-arm dynein. *J. Cell Sci.* 103:653–664.
10. Perrone, C. A., S. H. Myster, R. Bower, E. T. O'Toole, and M. E. Porter. 2000. Insights into the structural organization of the I1 inner arm dynein from a domain analysis of the 1beta dynein heavy chain. *Mol. Biol. Cell.* 11:2297–2313.
11. Habermacher, G., and W. S. Sale. 1997. Regulation of flagellar dynein by phosphorylation of a 138-kD inner arm dynein intermediate chain. *J. Cell Biol.* 136:167–176.
12. Smith, E. F., and W. S. Sale. 1991. Microtubule binding and translocation by inner dynein arm subtype I1. *Cell Motil. Cytoskeleton.* 18: 258–268.
13. King, S. J., and S. K. Dutcher. 1997. Phosphoregulation of an inner dynein arm complex in *Chlamydomonas reinhardtii* is altered in phototactic mutant strains. *J. Cell Biol.* 136:177–191.
14. Brokaw, C. J., and R. Kamiya. 1987. Bending patterns of *Chlamydomonas* flagella: IV. Mutants with defects in inner and outer dynein arms indicate differences in dynein arm function. *Cell Motil. Cytoskeleton.* 8: 68–75.
15. Sakakibara, H., H. Kojima, Y. Sakai, E. Katayama, and K. Oiwa. 1999. Inner-arm dynein c of *Chlamydomonas* flagella is a single-headed processive motor. *Nature.* 400:586–590.
16. Vallee, R. B. 1986. Reversible assembly purification of microtubules without assembly—promoting agents and further purification of tubulin, microtubule-associated proteins, and MAP fragments. *Methods Enzymol.* 134:89–104.
17. Burgess, S. A., M. L. Walker, H. Sakakibara, P. J. Knight, and K. Oiwa. 2003. Dynein structure and power stroke. *Nature.* 421: 715–718.
18. Burgess, S. A., M. L. Walker, H. Sakakibara, K. Oiwa, and P. J. Knight. 2004. The structure of dynein-c by negative stain electron microscopy. *J. Struct. Biol.* 146:205–216.
19. Walker, M. L., S. A. Burgess, J. R. Sellers, F. Wang, J. A. Hammer III, J. Trinick, and P. J. Knight. 2000. Two-headed binding of a processive myosin to F-actin. *Nature.* 405:804–807.
20. Frank, J., M. Radermacher, P. Penczek, J. Zhu, Y. Li, M. Ladjadj, and A. Leith. 1996. SPIDER and WEB: processing and visualization of images in 3D electron microscopy and related fields. *J. Struct. Biol.* 116:190–199.
21. Webb, M. R. 1992. A continuous spectrophotometric assay for inorganic phosphate and for measuring phosphate release kinetics in biological systems. *Proc. Natl. Acad. Sci. USA.* 89:4884–4887.
22. Hancock, W. O., and J. Howard. 1998. Processivity of the motor protein kinesin requires two heads. *J. Cell Biol.* 140:1395–1405.
23. Howard, J., A. J. Hudspeth, and R. D. Vale. 1989. Movement of microtubules by single kinesin molecules. *Nature.* 342:154–158.
24. Oiwa, K., J. F. Eccleston, M. Anson, M. Kikumoto, C. T. Davis, G. P. Reid, M. A. Ferenczi, J. E. Corrie, A. Yamada, H. Nakayama, and D. R. Trentham. 2000. Comparative single-molecule and ensemble myosin enzymology: sulfoindocyanine ATP and ADP derivatives. *Biophys. J.* 78:3048–3071.
25. Kojima, H., M. Kikumoto, H. Sakakibara, and K. Oiwa. 2002. Mechanical properties of a single-headed processive motor, inner-arm dynein subspecies-c of Chlamydomonas studied at the single molecule level. *J. Biol. Phys.* 28:335–345.
26. Johnson, K. A. 1983. The pathway of ATP hydrolysis by dynein. Kinetics of a presteady state phosphate burst. *J. Biol. Chem.* 258:13825–13832.
27. Shiroguchi, K., and Y. Y. Toyoshima. 2001. Regulation of monomeric dynein activity by ATP and ADP concentrations. *Cell Motil. Cytoskeleton.* 49:189–199.
28. Toba, S., T. M. Gibson, K. Shiroguchi, Y. Y. Toyoshima, and D. J. Asai. 2004. Properties of the full-length heavy chains of *Tetrahymena* ciliary outer arm dynein separated by urea treatment. *Cell Motil. Cytoskeleton.* 58:30–38.
29. Leibler, S., and D. A. Huse. 1993. Porters versus rowers: a unified stochastic model of motor proteins. *J. Cell Biol.* 121:1357–1368.
30. Sellers, J. R., S. Umemoto, and G. Cuda. 1993. In vitro studies of determinants of smooth muscle mechanics. *Adv. Exp. Med. Biol.* 332: 267–276.
31. Cuda, G., E. Pate, R. Cooke, and J. R. Sellers. 1997. In vitro actin filament sliding velocities produced by mixtures of different types of myosin. *Biophys. J.* 72:1767–1779.
32. Warshaw, D. M., J. M. Desrosiers, S. S. Work, and K. M. Trybus. 1990. Smooth muscle myosin cross-bridge interactions modulate actin filament sliding velocity in vitro. *J. Cell Biol.* 111:453–463.
33. Nicastro, D., C. Schwartz, J. Pierson, R. Gaudette, M. E. Porter, and J. R. McIntosh. 2006. The molecular architecture of axonemes revealed by cryoelectron tomography. *Science.* 313:944–948.
34. Goodenough, U. W., B. Gebhart, V. Mermall, D. R. Mitchell, and J. E. Heuser. 1987. High-pressure liquid chromatography fractionation of *Chlamydomonas* dynein extracts and characterization of inner-arm dynein subunits. *J. Mol. Biol.* 194:481–494.
35. Mastronarde, D. N., E. T. O'Toole, K. L. McDonald, J. R. McIntosh, and M. E. Porter. 1992. Arrangement of inner dynein arms in wild-type and mutant flagella of *Chlamydomonas*. *J. Cell Biol.* 118:1145–1162.
36. Porter, M. E., J. Power, and S. K. Dutcher. 1992. Extragenic suppressors of paralyzed flagellar mutations in *Chlamydomonas reinhardtii* identify loci that alter the inner dynein arms. *J. Cell Biol.* 118: 1163–1176.
37. Ishikawa, T., H. Sakakibara, and K. Oiwa. 2007. The architecture of outer dynein arms *in situ*. *J. Mol. Biol* 368:1249–1258.
38. Toba, S., T. M. Watanabe, L. Yamaguchi-Okimoto, Y. Y. Toyoshima, and H. Higuchi. 2006. Overlapping hand-over-hand mechanism of single molecular motility of cytoplasmic dynein. *Proc. Natl. Acad. Sci. USA.* 103:5741–5745.
39. Hirakawa, E., H. Higuchi, and Y. Y. Toyoshima. 2000. Processive movement of single 22S dynein molecules occurs only at low ATP concentrations. *Proc. Natl. Acad. Sci. USA.* 97:2533–2537.
40. Rikmenspoel, R., and W. G. Rudd. 1973. The contractile mechanism in cilia. *Biophys. J.* 13:955–993.
41. Lindemann, C. B. 1994. A model of flagellar and ciliary functioning which uses the forces transverse to the axoneme as the regulator of dynein activation. *Cell Motil. Cytoskeleton.* 29:141–154.
42. Lindemann, C. B. 2002. Geometric clutch model version 3: The role of the inner and outer arm dyneins in the ciliary beat. *Cell Motil. Cytoskeleton.* 52:242–254.